ELSEVIER

Journal of Fluids and Structures 20 (2005) 235–253

JOURNAL OF FLUIDS AND STRUCTURES

www.elsevier.com/locate/jfs

Excited turbulent flow behind a square rib

P.K. Panigrahi[a,*], S. Acharya[b]

[a]Department of Mechanical Engineering, Indian Institute of Technology, Kanpur 208016, India
[b]Department of Mechanical Engineering, Louisiana State University, Baton Rouge, LA 70803, USA

Received 15 July 2002; accepted 21 October 2004
Available online 17 January 2005

Abstract

The effect of fundamental excitation on the reattaching shear layer developing behind a surface mounted square rib has been discussed. The individual contributions from the random and the coherent part of the turbulent fluctuations are calculated using the pattern recognition approach. Quadrant analysis is used to investigate the turbulent motion details, i.e. ejections, sweep, wallward interaction motions and outward interaction motions of the rib roughened shear layer. In doing so, an interesting and previously unreported behavior about the relationship between the ejection motions and non-Gaussian nature of the flow is observed. The large-scale ejection motions predominant in the outer edge of the shear layer contribute to the non-Gaussian higher order moments. With excitation, the shear layer reattachment moves upstream, and the X-momentum transport is enhanced in the near-wall region. The Reynolds stress correlation profile shows a distinct difference between the redeveloping boundary layer behind the rib and the flat plate boundary layer.

1. Introduction

Ribbed duct flows are encountered in a variety of practical applications, for example, turbine blade cooling and internally ribbed heat exchangers. The flow behind a surface mounted rib is essentially characterized by flow separation about one-rib-height upstream and reattachment nearly 5 to 6 rib-heights downstream of the rib. The separated shear layer past the rib has been shown (Panigrahi and Acharya, 1996; Acharya et al., 1991) to be dominated by coherent structures and it is expected that the flow and heat transport mechanisms would be largely influenced by the dynamics of these structures. Hasan (1992) observed that the downward motion of the reattaching shear layer is not continuous but that it reverses intermittently. Arnal and Friedrich (1991) from their large eddy simulation of backward facing step flow observed large departures of the instantaneous flow field from the mean flow field and concluded that for a complete understanding of the reattaching shear flow, the instantaneous flow structure is required. Nearly all the reported measurements (Antonia and Luxton, 1971; Tropea and Gackstatter, 1985; Liou and Kao, 1988; Durao et al., 1991; Myrum et al., 1993) that have presented Reynolds stresses and heat fluxes in ribbed ducts, have done so without carefully identifying the mechanisms associated with the production and transport of these fluxes. Yet this information is critical, not only in understanding the basic flow mechanisms, but also in developing suitable models for turbulent transport. For turbulence modeling, the measurements of the time-averaged turbulent shear stresses have been used to

*Corresponding author. German Aerospace Center, Institute of Aerodynamics & Flow Technology, Bunsenstrasse 10, Goettingen 37073, Germany. Tel.: +91 512 2597686; fax: +91 512 2590007.
E-mail addresses: panig@iitk.ac.in, extern.panigrahi@dlr.de (P.K. Panigrahi).

0889-9746/$ - see front matter © 2004 Elsevier Ltd. All rights reserved.
doi:10.1016/j.jfluidstructs.2004.10.004

Nomenclature

A	amplitude
D_h	hydraulic diameter of the channel $(2WH/(W+H)) = 0.101$ m
U_f	power spectral density $\left(\equiv (1/T)\left(\left\|(T/N)\sum_{n=1}^{N} U(n)\mathrm{e}^{-2\pi ikn/N}\right\|\right)^2;\ k = 0, 1, 2, \ldots, N/2\right)$
h	rib height
H	height of the channel $= 0.061$ m
H_s	hole size
N	total number of samples
Re	Reynolds number
St	Strouhal number
T	total sampling time
u, v	streamwise and cross-stream velocity
u', v'	streamwise and cross-stream fluctuating velocity
t	time
W	width of the channel (0.3 m)
X	distance from the downstream edge of the rib in streamwise direction
Y	distance from channel bottom surface in wall normal direction
θ	momentum thickness $\equiv \int_0^{\delta}(1-u/U)(u/U)\,\mathrm{d}y$
μ	dynamic viscosity
ϕ	phase

Subscript

max	maximum
av	average
rms	root mean square
coh	coherent
rand	random
ref	reference

guide the development of turbulence models. However, the use of time-averaged measurements alone, without any reference to the flow structures and their motions, may be inadequate in developing universal models. Based on studies reported for perturbed shear layers (Ho and Huere, 1984), it is expected that superimposing an external excitation on the reattaching shear layer would promote mixing and shear layer growth. However, the selection of proper excitation parameters requires the complete understanding of turbulent structures and their evolution in the reattaching shear layer. Therefore, the detailed investigation of turbulent structures of a rib-roughened boundary layer and the influence of controlled excitation is the focus of this work.

The main scope of this work is to characterize the detailed turbulent motion of the flow behind a surface-mounted rib and the effect of controlled perturbation. The quadrant analysis technique is used to characterize the different types of eddy motion, i.e. ejection, sweep, wallward interaction motion and outward interaction motion and their contribution toward the production of turbulent normal stresses and turbulent shear stresses. The pattern recognition technique is used to extract the contribution of the coherent and random part of the turbulent fluctuation. The effect of excitation on the magnitude and scale of quadrant motions is presented. The quadrant analysis results are correlated with the higher-order moment calculations, i.e. skewness and flatness. In so doing an interesting and previously unreported relationship between the non-Gaussian nature of the flow field and quadrant motions is observed. The mean flow field, modal development, power spectrum and Reynold stress results are reported to provide a complete understanding of the turbulent flow field.

2. Description of experiment

The schematic of the experimental set-up is shown in Fig. 1. Air is drawn into a rectangular channel of 0.3 m × 0.06 m cross-section through a 5.25 to 1 contraction section, honeycomb and wire-mesh screens by a blower operating in the suction mode. Following the channel test-section is a settling chamber designed to eliminate swirl and large-scale turbulence generated by the blower. The free-stream turbulence at the exit of the contraction section is 0.4%. The Reynolds number based on the average velocity and hydraulic diameter of the channel is set equal to 14 600. The rib size (6.35 mm square rib cross-section) used here satisfies the two-dimensional flow criterion since the ratio of channel width to rib height is 47.2, which is larger than the required aspect ratio (12) to minimize three-dimensional affects (Antonia and Luxton, 1971). The blockage ratio with this test arrangement is 9.5%. At Re = 14 600, the thickness of the boundary layer developing on the bottom surface of the smooth channel (without the rib) at the rib location is 6 mm and the shape factor of this boundary layer is equal to 1.417. To investigate the state of the approaching flow, the velocity profile at the bottom surface of the channel without the rib, but at same location where the rib is placed, were

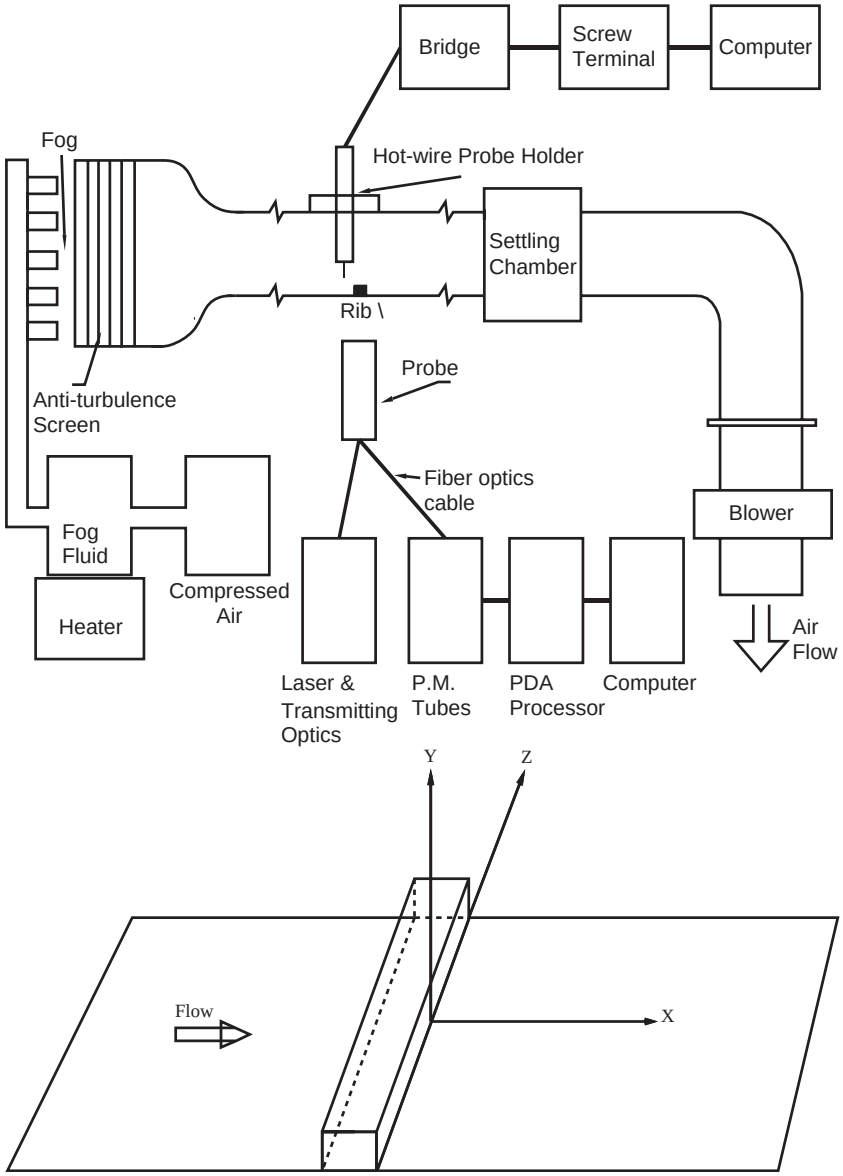

Fig. 1. Schematic of the experimental setup (top) and coordinate system of the rib (bottom).

compared with that of laminar (Blasius) and turbulent (Law of the wall) profile. The almost perfect match between the experiment and the law of the wall confirmed that the approach flow is turbulent.

Both hot-wire anemometry (X-wire) and two-component laser-Doppler velocimetry (LDV) were used for the velocity measurements. The hot-wire anemometer was operated in the constant temperature mode with a 70% overheat ratio. The anemometer output was connected to a Keithley Metrabyte data acquisition card (DAS-16) through a screw terminal accessory board (STA-16). The Streamer package supplied by Keithley Metrabyte was used to enable direct storage of data from the DAS-16 board to the hard disk of the computer. The hot-wire was calibrated using Model 1125 calibrator supplied by TSI. The calibration accuracy was confirmed by comparing the data taken by the hot-wire and the data taken using laser-Doppler anemometry, and the results of the mean velocities from the two different techniques were within one percent. The hot-wire data acquisition rate was 4160 Hz/channel and the total number of samples per channel was 16 384. External excitation of the flow was provided by using a loudspeaker driven by a function generator. The voltage input to the loudspeaker was simultaneously collected with the two channel output from the X-wire. Thus, the total sampling rate was 12.48 kHz and total number of samples for a single point measurement was 48k.

The laser-Doppler velocimetry measurements were performed using a two-color DANTEC fiber-optic LDV system. The argon-ion laser beam was split into a pair of 488 nm (blue) and 514.5 nm (green) wavelength beams using a color separator and a beam splitter. One beam from each of the two pairs was shifted by 40 MHz using a Bragg cell to eliminate the directional ambiguity in the velocity measurements. A 400 mm focal length lens focused the resulting pair of beams to a measurement volume of less than 0.2 mm waist diameter. The flow was seeded with an aerosol mist obtained by heating a fog fluid supplied by Rosco Inc. Backscattered light was collected by photomultiplier tubes and processed using the PDA signal processor and SIZEware software supplied by Dantec. The sampling rate of the LDV signal varied depending on the rate of supply and diameter of the seeding particle and was within the range of 100–2000 Hz. The total number of samples per point for averaging the LDV signal was 10 000. The reattachment length was measured by measuring the velocity at a location close to the bottom wall (2 mm away from the surface) at various streamwise locations (X/h). The location where the streamwise velocity changed sign from a negative value to a positive value was termed as the reattachment point. From the LDV measurements, it was observed that at the transverse locations, where $U/U_{\max}$ is greater than 0.65 the reversed flow intermittency is always zero ($U_{\max}$ here is defined as the maximum streamwise velocity at the corresponding X/h location). Therefore, the hot-wire measurements were made at or above the transverse location where $U/U_{\max} = 0.65$.

For exciting the flow, an arrangement similar to that of Fiedler and Mensing (1985) in their study of plane turbulent shear layer excitation was used. A two-channel PCI-312 signal generator from PC Instruments provided the necessary sinusoidal signal to the loudspeaker through a power amplifier from velodyne acoustics (Model OLD-12-N). The loudspeaker was connected to a rectangular cavity of dimension 0.5969 m × 0.3048 m × 0.0222 m. Styrofoam was mounted on the wall of the cavity, opposite to the loudspeaker, to minimize the effect of multiple reflection of acoustic waves inside the cavity. The acoustic wave is directed at an angle of 90° through a 4.76 mm wide slot. The slot is located 9-rib heights upstream of the rib and well ahead of the upstream recirculation region. The excitation frequency selected here is 52 Hz and is equal to the fundamental frequency measured in the unforced reattaching shear layer (see Fig. 2).

The forcing level is defined here as the normalized free-stream ($Y/h = 2.0$) r.m.s. velocity ($\overline{(u'^2)}^{1/2}/U_{\mathrm{av}}$) at the downstream edge of the rib ($X/h = 0$). The $Y/h = 2.0$ location represents the external free stream at the downstream edge of the rib. Different forcing levels were obtained by adjusting the voltage input to the power amplifier of the loudspeaker. To select the forcing level for this study, the momentum thickness at $X/h = 8$ was examined for different forcing levels. In selecting the optimum forcing level, it is desired to obtain the largest enhancements in mixing (or shear layer spreading) with the minimum level of energy input into the loudspeaker. It was observed that the rate of increase in momentum thickness which is proportional to the shear layer spreading reduces after the forcing level reaches 2%. Therefore, the 2% forcing level is considered as the optimum forcing level and this forcing level is used in this study.

2.1. Uncertainty

Basic equations of uncertainty described by Moffat (1982) have been used to calculate the uncertainty in the experimental results. The uncertainty in the X-wire and the LDV measurements are estimated to be ±0.01 and ±0.03 m/s, respectively. The uncertainty of the spatial location (X, Y) measurements is estimated to be the least count of the traverse mechanism (equal to 0.1 mm). The uncertainty in the momentum thickness and the Strouhal number based on momentum thickness are equal to 7.1% and 8.0%, respectively. The uncertainty of the most amplified frequency estimated as the spectral resolution of the power spectrum (reciprocal of signal observation time in second) is about 1.0 Hz. The most amplified frequency from repeated measurements being within 1 Hz of each other confirms the maximum uncertainty of spectrum to be less than 1 Hz. The uncertainty in the reattachment length from several repetitions of the experiments designed to measure the reattachment point is estimated to be 4%.

The uncertainty of the turbulent statistics i.e. u_{rms}, v_{rms}, $\overline{-u'v'}$, skewness ($\overline{u'^3}/\overline{(u'^2)}^{3/2}$) and flatness ($\overline{u'^4}/(\overline{u'^2})^2$) is due to the combination of calibration error, digitization error and proper selection of sampling frequency and sampling period. The sampling frequency and total number of samples in our experiment are, respectively, 2000 Hz and 16 384, which have been selected based on the frequency content of the velocity signal; these statistics are insensitive to any further increase in the sampling frequency and sampling period. From the standard deviation of the repeated measurements, the uncertainty in the u_{rms}, v_{rms}, $\overline{-u'v'}$, $\overline{u'^3}/\overline{(u'^2)}^{3/2}$ and $\overline{u'^4}/(\overline{u'^2})^2$are, respectively, estimated to be equal to 2.5%, 3.0%, 3.5%, 4% and 4.5%. The uncertainty in the coherent component of the above turbulent statistics is higher, due to the assumption in the coherent mode frequency and calculation of the Fourier amplitudes. The uncertainty of the coherent components, u_{coh}, v_{coh}, $\overline{-u'v'}_{\mathrm{coh}}$, $(\overline{u'^3}/\overline{(u'^2)}^{3/2})_{\mathrm{coh}}$ and $(\overline{u'^4}/(\overline{u'^2})^2)_{\mathrm{coh}}$ are, respectively, estimated as 3.5%, 4.0%, 4.5%, 5.0% and 5.5%. The uncertainty in the Reynolds stress correlation ($\overline{u'v'}/u_{\mathrm{rms}}v_{\mathrm{rms}}$) is equal to 4.5%. The uncertainty in the average hole size is due to the combination of the error in Reynolds stress measurement and the integration error during calculation, which is estimated to be equal to 5.0%.

3. Data analysis

The contribution of the coherent component of the fluctuating velocity signal is obtained by the pattern recognition technique. The contribution of the coherent fluctuation towards the shear stresses, normal stresses and higher order moments, i.e. skewness and flatness are presented. The presence and significance of different turbulent motions, i.e. ejections, sweep, outward interaction motion and wallward interaction motion are examined from using the quadrant analysis. These two data analysis techniques are discussed below.

3.1. Pattern recognition technique

The contribution to the total velocity fluctuation comes from both the random and coherent eddies. The pattern recognition technique helps to calculate these individual contributions. In this technique, the coherent velocity component is approximated to be the combined contribution from several modes. To identify the dominant modes present in the reattaching shear layer behind the rib, the power spectral density of the u-velocity at different X/h locations is presented in Figs. 2 and 3 for the unexcited and excited cases, respectively. The fundamental and subharmonic modes are clearly observed to be the dominant modes. The $\frac{3}{2}$ fundamental may however be present due to the non-linear interaction between the fundamental and its subharmonic. Similarly, the $\frac{5}{2}$ fundamental may result due to the non-linear interaction between the $\frac{3}{2}$ fundamental and the fundamental. Thus, assuming the coherent velocity to be the combination of the fundamental, the 1st subharmonic, the 2nd subharmonic, the 3rd subharmonic, the 1st harmonic, the $\frac{3}{2}$ fundamental and the $\frac{5}{2}$ fundamental, the coherent velocity component can be written as

$$u_c(x,y,t) = \sum_k A_k(x,y)\cos(k\omega_f t + \phi_k(x,y,t)), \quad k = \tfrac{1}{4}, \tfrac{1}{2}, 1, 2, 3, 4, 5, \tag{1}$$

where ω_f is the 1st subharmonic frequency (equal to half the forced frequency or natural frequency), A_k and ϕ_k are the amplitude and phase corresponding to the respective mode and $k = \frac{1}{4}, \frac{1}{2}, \ldots, 5$ represent, respectively, the 3rd

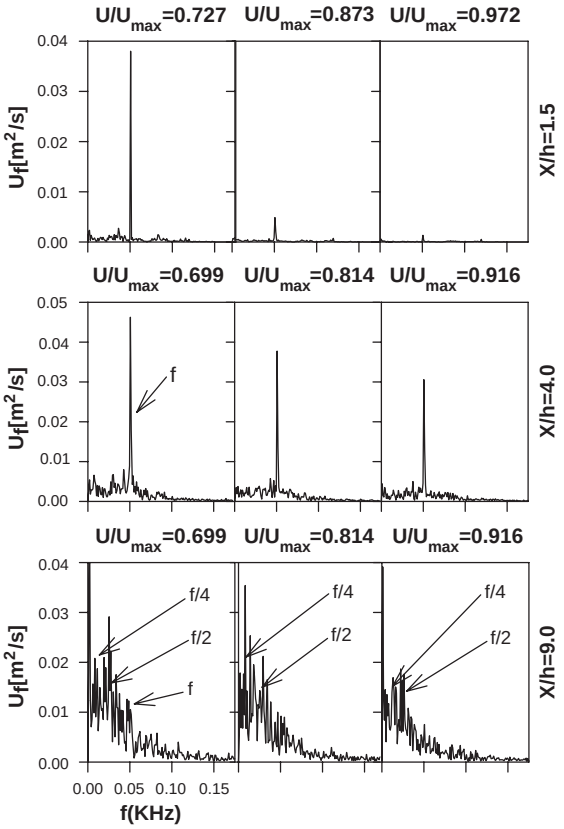

Fig. 2. The power spectral density of the streamwise u-velocity for the unexcited flow behind the rib.

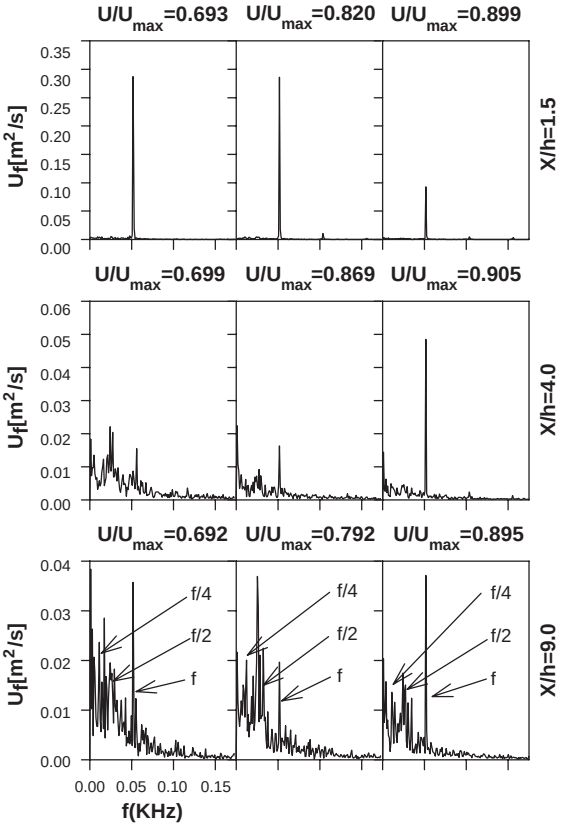

Fig. 3. The power spectral density of the streamwise u-velocity for the excited flow behind the rib.

subharmonic, the 2nd subharmonic, the 1st subharmonic, the fundamental, the $\frac{3}{2}$ fundamental, the harmonic and the $\frac{5}{2}$ fundamental. For modes having phase jitter, the ϕ_k values are not constant from one period of the mode to the other. Any contribution from frequency larger than the maximum frequency (here the $\frac{5}{2}$ fundamental) will be regarded as coming from the random small-scale motion. Any contribution below the minimum frequency considered (the 3rd subharmonic here) will appear in the zeroth coefficient of the Fourier series and represents the jitter of the mean velocity per segment.

The evaluation of the Fourier components for different modes is performed by segmenting the whole time series of the signal into different segments, such that, in one segment, one period of the corresponding wave is present. The total mean of the time series is subtracted from the signal first. Then the calculation of the Fourier components is performed starting with the lowest frequency using segments that exactly contain one wave of this mode. Thus for the 3rd subharmonic, segments used are eight fundamental waves long, for the 2nd subharmonic the segments are four fundamental waves long, and so on. Prior to the computation of each subsequent mode, the computed contribution from the previous mode is subtracted from the remaining signal. This avoids erroneous contributions from the previous modes. Time periods equal to twice that of the fundamental are used to evaluate the $\frac{3}{2}$ fundamental, the $\frac{5}{2}$ fundamental and the subharmonic. For the $\frac{3}{2}$ fundamental and $\frac{5}{2}$ fundamental, segments of 1.5 times the fundamental time period and 0.4 times the fundamental time period cannot be used, because the respective calculated magnitude will be affected by the fundamental wave. Segments equal to the fundamental time period also cannot be used as the segment will not contain a whole number of waves of $\frac{3}{2}$ fundamental and $\frac{5}{2}$ fundamental frequency. Therefore, the segment of length equal to twice the fundamental time period is used. The $\frac{3}{2}$ fundamental and $\frac{5}{2}$ fundamental wave amplitudes and phases are calculated first from these segments, and then their contributions are subtracted from the time series before computing the 1st subharmonic. After subtracting the contribution of 1st subharmonic the calculation of fundamental and 1st harmonic are performed using segments of length equal to one period of the fundamental wave. The total coherent structure amplitude is calculated by summing the amplitudes of all modes ($\frac{5}{2}$ fundamental, 1st harmonic, $\frac{3}{2}$ fundamental, fundamental, 1st subharmonic, 2nd subharmonic and 3rd subharmonic). It should be noted that the

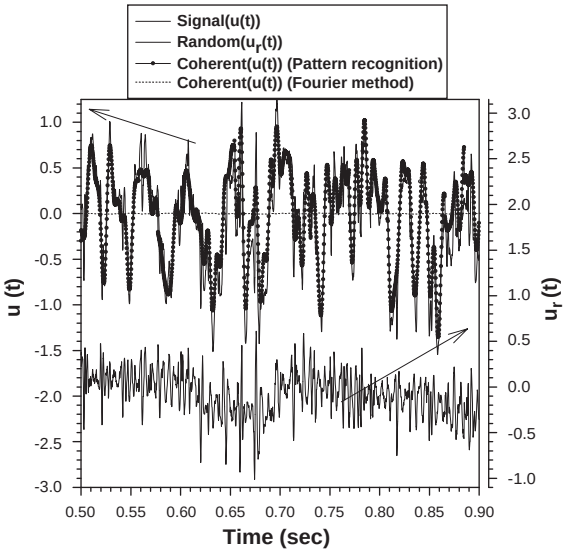

Fig. 4. The coherent (using pattern recognition and Fourier method) and random component (using pattern recognition method) of the velocity signal at $X/h = 4.0$ and $U/U_{\max} = 0.7$ location for forced reattaching shear layer.

choice of frequencies to be included in the definition of coherent structures should be based on the predominant modes present in the turbulent signal. The non-inclusion of predominant modes will result in over-predicting the turbulent part and under-predicting the coherent part. Sample results of the coherent contribution inside the forced reattaching shear layer using traditional Fourier technique and pattern recognition technique is shown in Fig. 4. The pattern recognition technique is observed to perform satisfactorily while the Fourier technique underpredicts the coherent magnitude.

3.2. Quadrant analysis

Quadrant analysis has been successfully used in flat plate boundary layer flows by several investigators (Wallace et al., 1972; Willmarth and Lu, 1972; Bogard and Tiederman, 1987; Luchik and Tiederman, 1987) for predicting the types of turbulent motion and the scales contributing to these motions. Volino et al. (1994) used an extended quadrant analysis technique for heated flows known as the octant analysis to study the turbulent and transitional boundary layer on heated flat and curved surfaces. Panigrahi and Acharya (1999) used a modified octant analysis technique to study the turbulent motions behind a surface mounted rib. The turbulent motions are identified as: (i) low-speed fluid moving away from the wall, called *ejections* ($u'<0, v'>0$), (ii) high-speed fluid moving toward the wall, called *sweep* ($u'>0, v'<0$), (iii) high-speed fluid pushed away from the wall as *outward interaction* ($u'>0, v'>0$), and (iv) low-speed fluid being pushed back toward the wall as *wallward interaction* ($u'<0, v'<0$). The quadrant analysis technique is used here to investigate the types of turbulent motions responsible for non-Gaussian skewness and flatness values at the outer edge of the shear layer and to investigate the effect of excitation on the total contribution and scales of different turbulent motions.

The different turbulent motions, i.e. ejection, sweep, outward interaction and wallward interaction, representing the four quadrants in the $u'v'$ plane can be further partitioned based on the strength of the eddies. Eddies of certain strength, characterized by the hole size H_s, can be identified by computing their contribution to $\overline{u'v'}$ when the signal $|u'v'|$ is greater than the value $H_s|u'v'|_{\text{ref}}$, where, $|u'v'|_{\text{ref}}$ represents the maximum absolute shear stress at all locations considered ($X/h = 1.5$, 4.0 and 9.0). In the present study, $|u'v'|_{\text{ref}}$ is chosen to be the maximum Reynolds stress for all X/h and Y/h locations to allow consistent comparisons of eddy sizes between different locations. The contributions from different quadrants are calculated as a function of the hole size, and provide an estimate of the eddy sizes in each quadrant. For a consistent comparison of eddy sizes at different locations and for different quadrant motions, an average hole size is used. The average hole size is defined as

$$H_{s(\text{av})} = \int_0^\infty (u'v')\,\mathrm{d}H_s/(u'v')_{H_s=0}. \tag{2}$$

4. Results and discussion

The results are presented here in the following sequence: (1) power spectrum, (2) mean velocity, (3) Reynolds stresses, (4) higher-order moments and (5) quadrant analysis.

4.1. Power spectrum

Figs. 2 and 3 present the spectra of the streamwise velocity in the unforced flow and forced flow, respectively. Spectra at three X/h locations are shown; $X/h = 1.5$ corresponds to a location just downstream of the separation, $X/h = 4.0$ is a near reattachment location, and $X/h = 9.0$ is downstream of the reattachment point. The spectrums are also shown at three Y/h locations ($U/U_{\max} \simeq 0.7$, 0.8, 0.9) inside the shear layer. At $X/h = 1.5$ and $U/U_{\max} = 0.727$, the spectrum reveals the presence of a clear shear layer instability at about 52 Hz (fundamental). No other peaks are seen in this spectrum, indicating a relatively clean flow with low free stream turbulence and uncontaminated by other spurious frequencies arising from the blower or the honeycomb. The Strouhal number based on the momentum thickness at the downstream corner of the rib ($X/h = 0$) and average velocity of the channel is equal to 0.012. For a backward facing step, Hasan (1982) observed the Strouhal number based on momentum thickness to be equal to about 0.012. The Y/h

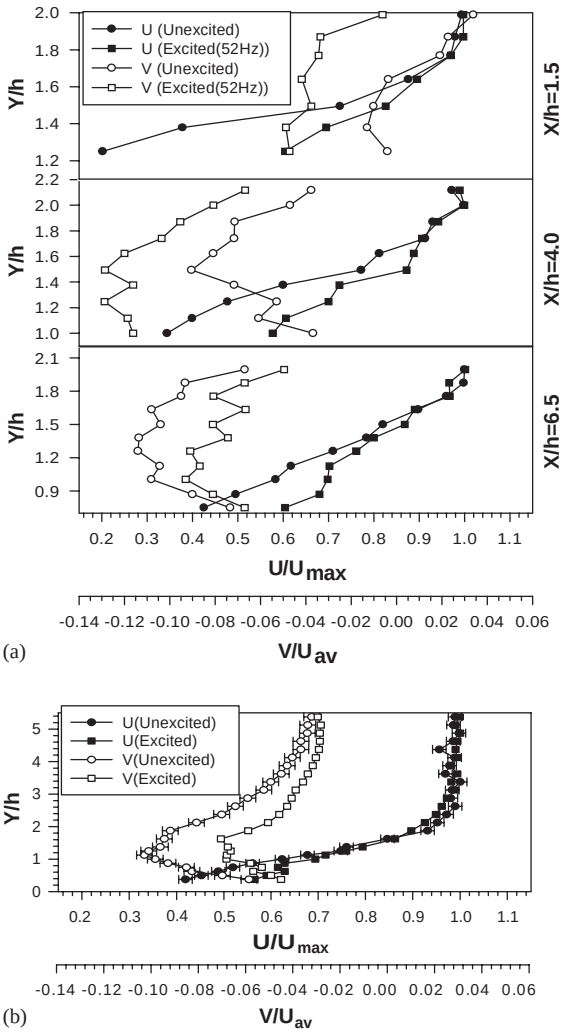

Fig. 5. Mean velocity profiles at (a) $X/h = 1.5$, 4.0 and 6.5 (near and upstream of reattachment location) and (b) at $X/h = 9.0$ (downstream of reattachment) for both excited and unexcited flow.

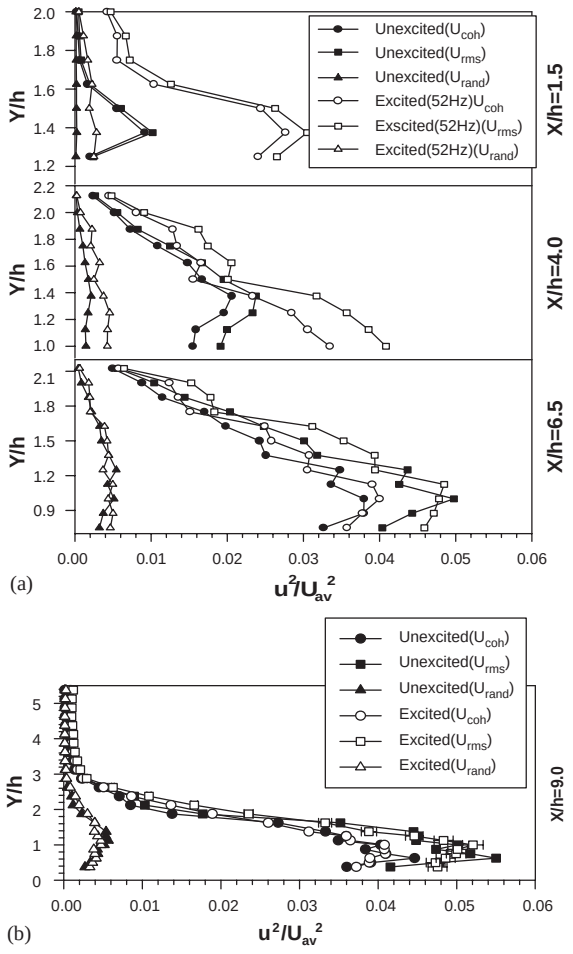

Fig. 6. Streamwise fluctuation profile at (a) $X/h = 1.5$, 4.0, and 6.5 (near and upstream of reattachment location) and (b) at $X/h = 9.0$ (downstream of reattachment) for both excited and unexcited flow.

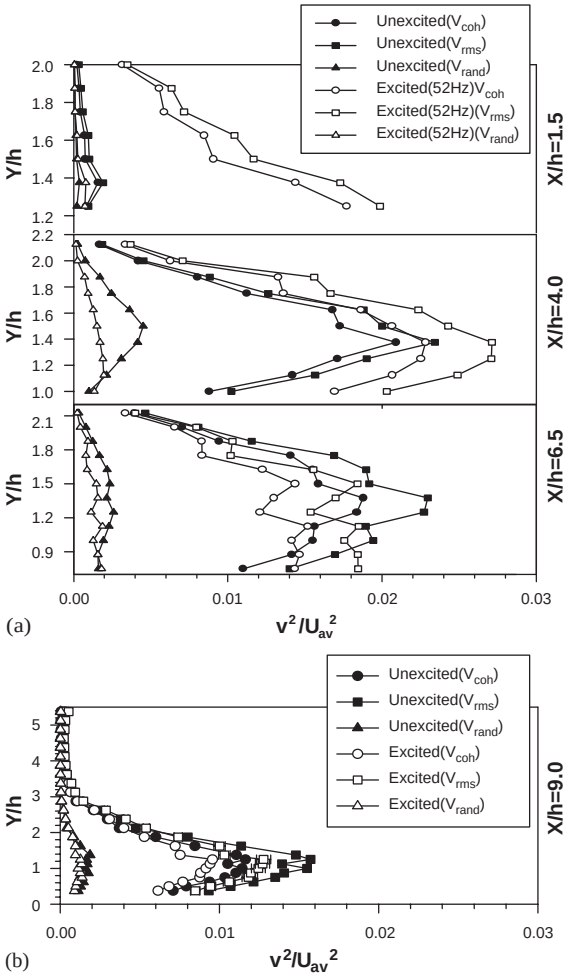

Fig. 7. Cross-stream fluctuation profile at (a) $X/h = 1.5$, 4.0, and 6.5 (near and upstream of reattachment location) and (b) at $X/h = 9.0$ (downstream of reattachment) for both excited and unexcited flow.

location where $U/U_{\max} = 0.972$ being away from the core of the shear layer, no clear spectral peak is observed in Fig. 2. At $X/h = 4.0$, the magnitude of the fundamental frequency has increased at all Y/h locations showing the growth of the most unstable frequency. As the flow develops, additional frequencies manifest themselves, and at $X/h = 9.0$, the fundamental has diminished considerably in magnitude, while the first and second subharmonic appear to have manifested themselves.

Fig. 3 shows the power spectral density for the excited flow. The magnitude of the fundamental peak at $X/h = 1.5$ is observed to be higher for the excited flow in comparison to that for the unexcited flow (Fig. 2). At $X/h = 4.0$ and $U/U_{\max} \simeq 0.7$ the fundamental peak for the excited flow has reduced in comparison to that for the unexcited flow indicating an earlier saturation of the fundamental mode. But, at $X/h = 4.0$ and $U/U_{\max} = 0.916$, the fundamental peak has higher magnitude than that at $X/h = 1.5$ indicating the continuation of fundamental mode growth. Hence, the saturation of the fundamental wave does not take place at same streamwise location along all cross-stream locations inside the shear layer. At $X/h = 4.0$ and $U/U_{\max} \simeq 0.7$, subharmonics have appeared for the excited flow, indicating early saturation of the fundamental mode. At $X/h = 9.0$, the spectra in Fig. 3 are similar to that of the unexcited flow, the relative modal magnitude of the fundamental and subharmonics being different from each other.

The most amplified frequency (fundamental mode) of the unexcited flow has highest growth rate among all the frequencies of the shear layer. Due to the superposed (fundamental) excitation, the initial amplitude of the most unstable mode in the shear layer increases. This leads to rapid growth of the fundamental mode and early saturation of

its magnitude. The growth rate of the subharmonic mode increases after the saturation of the fundamental mode. The comparison of the fundamental mode magnitude development between Figs. 2 and 3 confirms the early saturation of the fundamental mode. The early appearance of subharmonics at $X/h = 4.0$ for the excited flow (see Fig. 3) in comparison to that for the unexcited flow (see Fig. 2) also is a consequence of early fundamental mode saturation due to the imposed excitation. It has been observed in mixing layer studies that development of subharmonics correlates to the shear layer growth. Therefore, the early development of subharmonics for the excited flow leads to greater growth of the reattaching shear layer and subsequent reduction in the reattachment length. This observation has been confirmed from the measurements of reattachment length. The reattachment length for the excited flow drops about ($\simeq 1.5h$) in comparison to the unexcited flow.

4.2. Mean velocity

The mean streamwise velocity and cross stream velocity for both the excited and the unexcited flow are presented in Fig. 5. The u-velocity is normalized by the maximum velocity (U_{max}) at the corresponding X/h location, while the v-velocity is normalized with the average u-velocity (U_{av}) across the channel. The effect of forcing on the mean v-velocity is observed to be considerably more pronounced than on the u-velocity and manifests itself over the entire measurement region in the shear layer. This reflects the greater receptivity of the v-momentum to the imposed perturbation. At $X/h = 1.5$, the v-velocity is positive in the upper half of the unexcited separated shear layer resulting from the upward deflection of the shear layer. For the excited flow, the v-velocity is mostly negative at this location indicating a downward motion of the flow. This earlier transition to downward motion for the excited flow is an indicator of earlier reattachment. From the LDV measurements, the reattachment length for the unexcited flow is equal to $5.5h$ and for the excited flow is equal to $4.0h$ supporting the above observation.

Acharya et al. (1998) observed low heat transfer in the recirculation zone downstream of the rib. Therefore, reduction in the reattachment length indicates reduction in low heat transfer zone and enhancement in average heat transfer. At $X/h = 9.0$, the maximum absolute v-velocity value for the unexcited flow is 42% more than the excited flow. The smaller v-velocities for the excited flow is a manifestation of the earlier reattachment and a greater extent of boundary

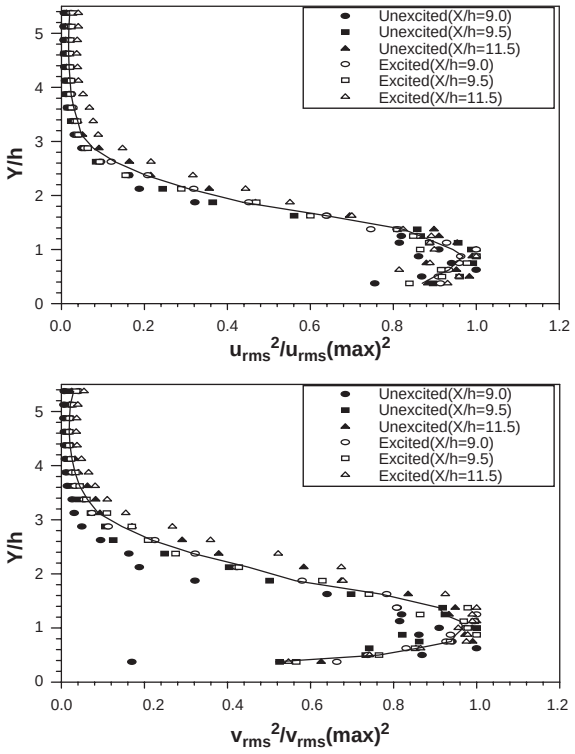

Fig. 8. Normalized streamwise (top) and cross-stream (bottom) fluctuations at various X/h locations for both excited and unexcited flow.

layer development. At $X/h = 1.5$, the effect of excitation on the mean u-velocity can be seen primarily upto a Y/h value of 1.5. For $Y/h > 1.5$, the u-velocity gradients are small, and no effect of excitation is observed. In the vicinity of reattachment and beyond ($X/h = 9.0$) the effect of excitation is limited to the near wall region only with higher momentum transport when the flow is excited.

4.3. Reynolds stresses

4.3.1. Normal stresses

The normal velocity fluctuations (streamwise and cross-stream) for both the excited and unexcited flow are plotted in Figs. 6 and 7, respectively at $X/h = 1.5$, 4.0, 6.5 and 9.0 . All stress values are normalized by the square of the average velocity in the channel. In the near-field region ($X/h = 1.5$ and 4.0), the streamwise and cross-stream fluctuations for the excited flow are considerably larger than those for the unexcited flow. However, the differences diminish in the downstream direction, and a cross-over occurs in the vicinity of reattachment. At $X/h = 6.5$, the near-wall streamwise and cross-stream fluctuation are higher for the excited flow in comparison to the unexcited flow. Higher value of v-fluctuation indicates enhanced heat transfer (Durbin and Reif, 2001) for the excited flow. In the far field region

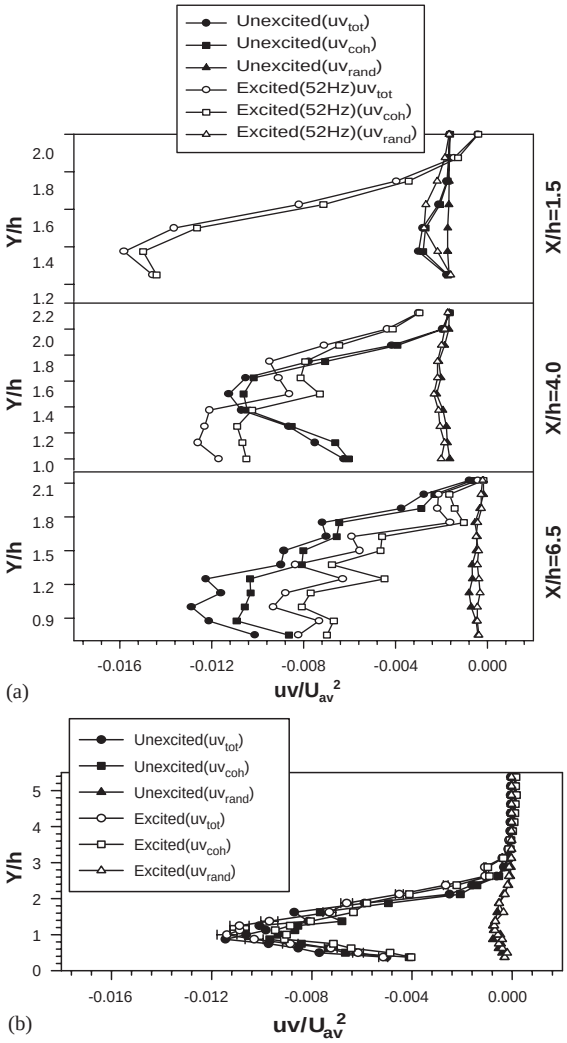

Fig. 9. Shear stress profile at (a) $X/h = 1.5$, 4.0, and 6.5 (near and upstream of reattachment location) and (b) at $X/h = 9.0$ (downstream of reattachment) for both excited and unexcited flow.

($X/h = 9.0$), the velocity fluctuations (streamwise and cross-stream) for the excited flow are smaller than those of the unexcited flow. This cross-over is due to the earlier saturation of the production of turbulent energy of the excited shear layer compared to that of the unexcited flow. For a backward facing step, Hasan (1992) also observed lower streamwise turbulence intensity after the reattachment region for the excited flow compared to the unexcited flow.

The contribution from the coherent fluctuation, calculated using the pattern recognition method are also shown in Figs. 6 and 7. Both before and after reattachment, the coherent components are significantly larger than the random components indicating that the large-scale eddies dominate the development of the reattaching shear layer. It may also be observed that the imposed oscillation mostly affects the coherent velocity fluctuations, while the random part is only indirectly affected by energy transfer mechanisms. The coherent velocity fluctuations are primarily affected by excitation because of the higher growth rate of the most unstable fundamental mode.

In the vicinity of reattachment ($X/h = 6.5$) and beyond ($X/h = 9.0$), the peak in the v-velocity fluctuation (see Fig. 7) can be observed to occur further away from the wall compared to the u-fluctuation (see Fig. 6). This is due to the stronger inhibiting effect of the solid surface on the v-fluctuation. Zhou et al. (1996), using the no slip condition and the continuity equation, argued that at the wall of a wall jet, both the v-fluctuation and the gradient of v-fluctuation are zero and therefore the influence of the wall is more pronounced in the v-fluctuation. The present study corroborates this argument, and due to this wall-damping effect, the peak in the v-fluctuation profile occurs at a higher Y/h value.

The u and v fluctuations profile normalized with respect to their maximum values are presented in Fig. 8 for various X/h locations downstream of reattachment. The normalized u_{rms} turbulent profiles collapse satisfactorily onto a single distribution with a maximum deviation of about 15% (see Fig. 8). However, the normalized v_{rms} turbulent profiles show larger deviations from the mean curve. Since, the differences in the reattachment location between the excited and unexcited flow is about $1.5h$, an assessment of the boundary layer development for the excited and the unexcited flow at the same location relative to the reattachment point can be made by comparing the u_{rms} and v_{rms} profiles at X/h of 9.5 for the excited flow (open rectangle) with the profiles at $X/h = 11.5$ for the unexcited flow (filled triangle). The agreement between these two sets of profiles is quite good, indicating that at downstream of reattachment both the unexcited and excited flows develop at the same rate.

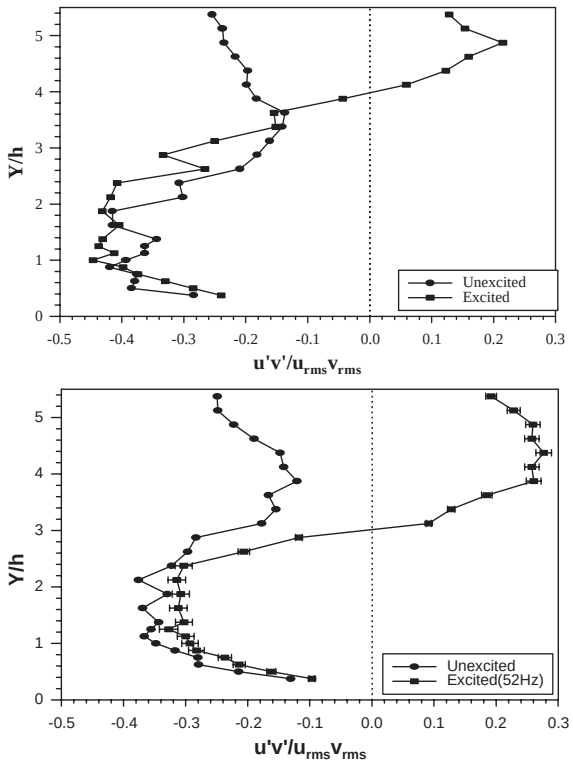

Fig. 10. Reynolds stress correlation for both excited and unexcited flow at $X/h = 9.0$ (top) and $X/h = 11.5$ (bottom).

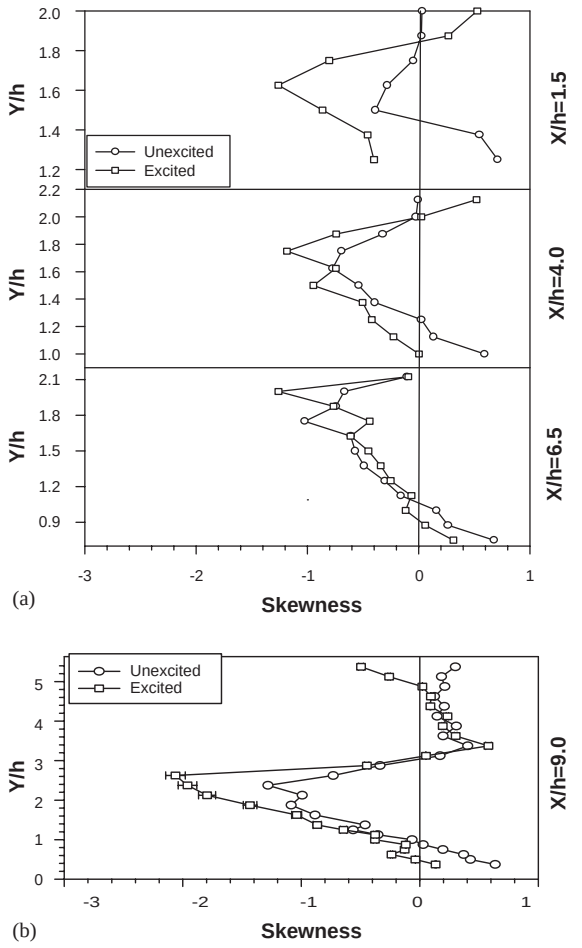

Fig. 11. The skewness of u-fluctuation at (a) $X/h = 1.5$, 4.0, and 6.5 (near and upstream of reattachment location) and (b) at $X/h = 9.0$ (downstream of reattachment) for both excited and unexcited flow.

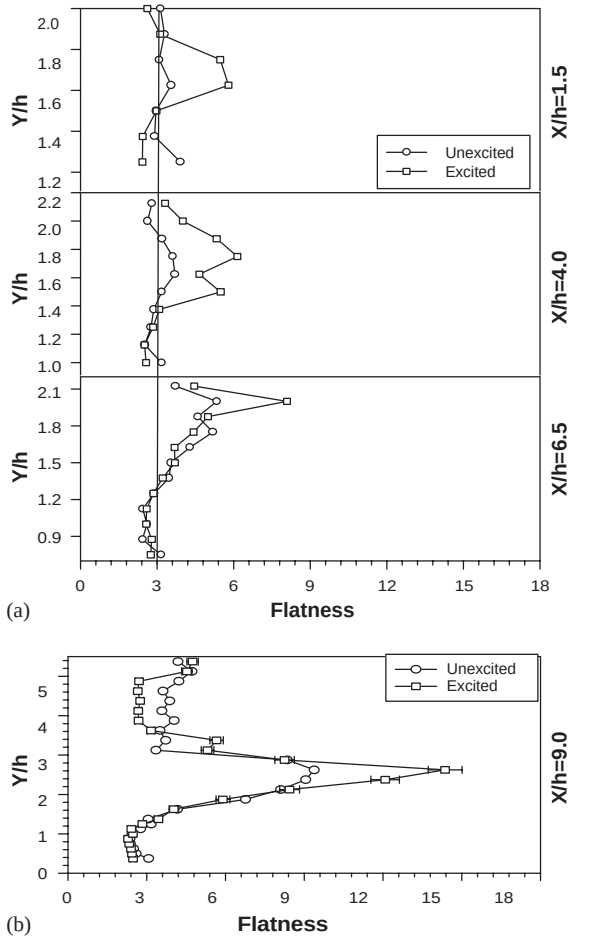

Fig. 12. The flatness of u-fluctuation at (a) $X/h = 1.5$, 4.0, and 6.5 (near and upstream of reattachment location) and (b) at $X/h = 9.0$ (downstream of reattachment) for both excited and unexcited flow.

4.3.2. Shear stresses

The evolution of the shear stress (coherent, total and random) at $X/h = 1.5$, 4.0, 6.5 and 9.0 are presented in Fig. 9. The effect of excitation is observed to be more pronounced in the near-field region. At $X/h = 6.5$, the shear stress for the excited flow is observed to be smaller than the unexcited flow. Thus, the turbulent shear stress in the vicinity of reattachment is less for the excited flow. As the flow recovers downstream of reattachment, the shear stress for the two cases become comparable (at $X/h = 9.0$). The excitation-induced reduction in shear stress between reattachment and $X/h = 9.0$, combined with a reduction in the reattachment length, points to the potential of using excitation for heat transfer enhancement (due to the smaller recirculation zone) with little drag penalty (due to excitation, a part of the flow has a reduction in shear stress while the other part has an increase in shear stress and these effects partly offset each other).

The Reynolds stress correlation ($\overline{u'v'}/(u_{\rm rms}v_{\rm rms})$) for both the unexcited and the excited flow in the post-reattachment region ($X/h = 9.0$ and 11.5) are presented in Fig. 10. The Reynolds stress correlation is an indication of the measure of momentum transport across the boundary layer (Zhou et al., 1996). The maximum value of the Reynolds stress correlation at $X/h = 9.0$ for both the excited and unexcited flow is about 0.46 and occurs in the range $1.0 < Y/h < 2.4$. The maximum shear stress occurs at $Y/h \simeq 1.4$ (see Fig. 9). Hence, there is efficient momentum transport across the major portion of the shear layer. This may be due to the predominant ejection motions present along the outer edge of the shear layer (discussed in the following section). The maximum value of the Reynolds stress correlation at

$X/h = 11.5$ is about 0.38 for the unexcited case and 0.32 for the excited case. For the unexcited flow behind the backward facing step, Chandrasuda and Bradshaw (1981) observed the shear layer correlation to be equal to 0.47 near the reattachment region which subsequently falls to about 0.4 after reattachment, with no sign of recovery to the usual boundary layer value of 0.45–0.5. A similar drop in the correlation value after reattachment is observed for the present flow with the exception that the drop in the correlation value for the excited case is larger than the unexcited case. For the excited case, the u-velocity profile develops faster and is therefore associated with a larger drop in correlation value. The correlation value never recovers to that of a flat plate boundary layer. Therefore, it may be concluded that the redeveloping boundary layer after reattachment behind the rib and the traditional flat plate boundary layer are not similar.

4.4. Higher-order moments

The higher order correlations, skewness $(\overline{u'^3}/(\overline{u'^2})^{3/2})$ and flatness $(\overline{u'^4}/(\overline{u'^2})^2)$ are presented for both the excited and the unexcited flow in Figs. 11 and 12. Much of the information missing from the conventional statistical descriptions may be found in the third and fourth moments. Outside the shear layer, the skewness has a Gaussian value, close to zero (see Fig. 11), indicating the symmetry of the fluctuation about the local mean velocity. The skewness in the upper part of the shear layer is significantly different from the Gaussian value. The maximum absolute value of skewness is higher for the excited flow and occurs at a higher Y/h location. The Y/h location corresponding to maximum skewness value increases in the downstream direction and is due to the increase in the boundary layer growth (see Fig. 5). The flatness has maximum offset from the Gaussian value of 3.0 at the same Y/h location where the skewness has maximum deviation from the Gaussian value (see Figs. 11 and 12). Comparing Figs. 6, 11 and 12, it can be observed that the highest values of the coherent and r.m.s. fluctuations occur at the Y/h location where the skewness and flatness values are about 0 and 3, respectively. This indicates that the flow structures in the high turbulent intensity region have Gaussian distributions.

Comparing Figs. 11 and 12 with Figs. 6 and 7, it may be observed that the Y/h locations having non-Gaussian distribution (higher value of skewness and flatness) corresponds to the upper part of the shear layer, that is in the region

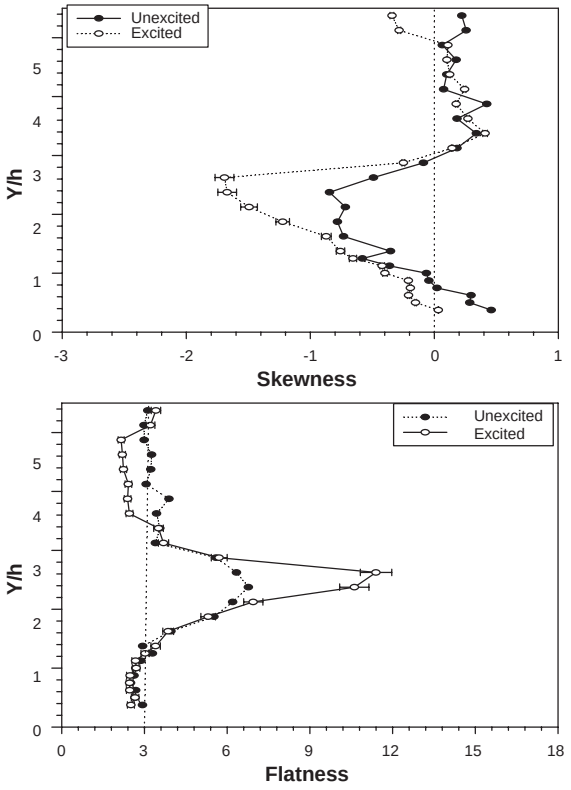

Fig. 13. Skewness(top) and flatness(bottom) profile of the coherent u-velocity for both unexcited and excited flow at $X/h = 9.0$.

contained between the location of maximum turbulence intensity to the edge of the shear layer. In the upper part of the shear layer, as will be shown later, large-scale ejection of low-momentum fluid takes place near the interface. These intermittent large scale ejection motions are the primary cause for the higher value of skewness and flatness at these locations. The skewness and flatness from the coherent part of the velocity signal has been shown in Fig. 13. The highest offset in the skewness and flatness value is observed to occur at the same Y/h location for the coherent velocity signal as for the total velocity signal. Further, the difference in the skewness and flatness value between the total and the coherent components is insignificant. This implies that the intermittent velocity fluctuation along the edge of the shear layer is mostly from low frequency large-scale fluctuations and not from small-scale eddies.

4.5. Quadrant analysis

The contributions from the different turbulent motions for the unexcited flow at $X/h = 1.5$, 4.0 and 9.0 are presented in Fig. 14. At $X/h = 1.5$, the total turbulent stress contribution comes primarily from the ejection and sweep motions. At $X/h = 4.0$ and 9.0, the ejection motion has a higher contribution at the outer edge of the shear layer, while the sweep motion has a larger contribution closer to the wall. The stress reducing motions (outward and wallward interactions) are smaller than the sweep and ejection motions, and range from nearly 30% of $\overline{u'v'}$ near the wall to less than 2% around $Y/h = 1.5$. These values are consistent with those for a flat plate boundary layer flow with the exception that contributions from wallward interactions are smaller.

For the forced flow, the contributions from different turbulent motions at $X/h = 1.5$, 4.0 and 9.0 are presented in Fig. 15. At $X/h = 1.5$, the stress producing motions are much stronger than the stress reducing motions thus resulting in a high values of the shear stress. The total contributions from the various turbulent motions are much larger for the

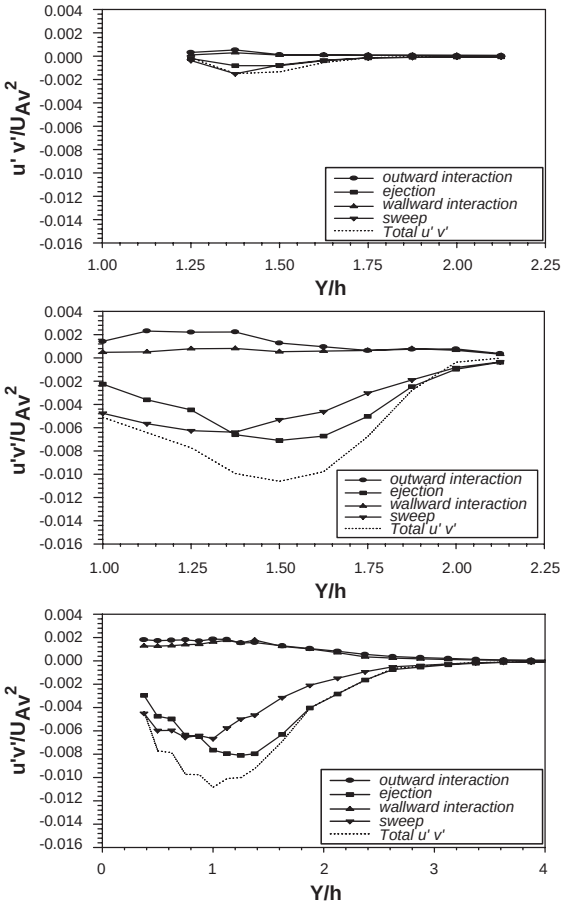

Fig. 14. The turbulent contribution profile (uncertainty = ±4.5%) of different quadrants at $X/h = 1.5$ (top), 4.0 (middle) and 9.0 (bottom) for the unexcited flow.

excited flow (Fig. 15) compared to that for the unexcited flow (Fig. 14). Most of the contributions to the total shear stress are from the ejection and sweep motions. The wallward and outward interaction motions are not much affected by the excitation. At $X/h = 4.0$, the ejection motion is stronger than the sweep motion at all Y/h locations, and the outward interaction motion is stronger than the wallward interaction motion. The maximum sweep motion contribution decreases from $X/h = 1.5$ to 4.0 location, while the maximum outward interaction motion and the ejection motion increases. Consequently, the maximum shear stress at $X/h = 4.0$ is smaller than that at $X/h = 1.5$. From $X/h = 4.0$ to 9.0 there is a substantial decrease in the contribution of ejection, sweep and outward interaction motions. The outward interaction motion and wallward interaction motion are both small at $X/h = 9.0$ and most of the contributions to the total Reynolds stress is from the ejection and sweep motions.

The average hole sizes for the unexcited flow at $X/h = 1.5$, 4.0 to 9.0 are presented in Fig. 16. The maximum average hole size for all motions increases in the downstream direction reflecting an increase in the size of the coherent structures. Among all the motions, ejection is associated with the largest-scale eddies. For each turbulent motion, it may be observed that the larger hole sizes (large-scale structures) are also associated with larger contributions to the shear stress (containing the most energy). It should be noted that the large magnitude of the coherent structures obtained using the pattern recognition method in the previous section also supports the above observation.

The average hole size profile for the excited flow at $X/h = 1.5$, 4.0 and 9.0 are shown in Fig. 17. Compared with the unexcited flow, the average hole size for the excited flow is observed to be higher at $X/h = 1.5$, indicating a greater growth of the large scales. At $X/h = 9.0$, the maximum average hole size of the ejection motion is smaller for the excited flow due to earlier saturation of the large-scale motions. This observation was also made earlier based on the magnitude of the streamwise velocity fluctuations, where the velocity fluctuations with excitation were lower than the velocity fluctuations without excitation near the reattachment point.

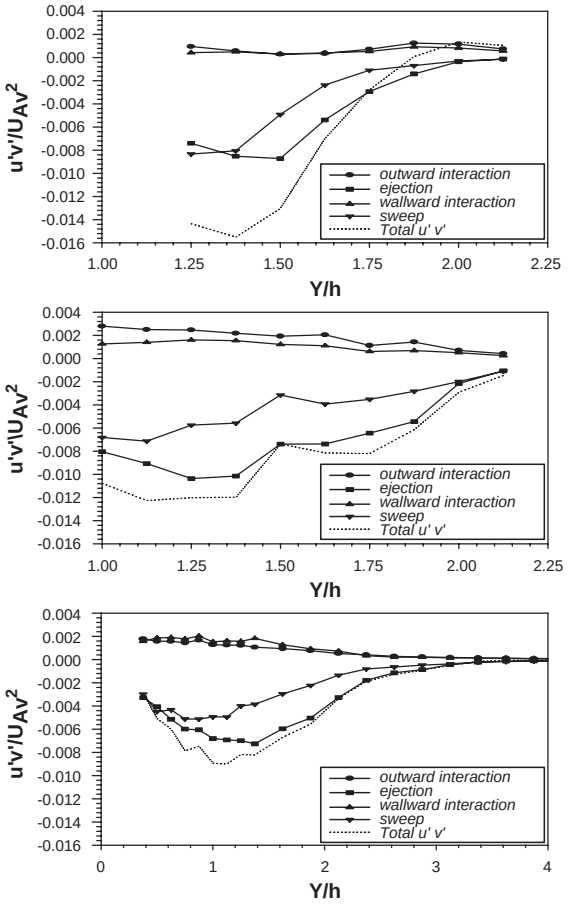

Fig. 15. The turbulent contribution (uncertainty = ±4.5%) profile of different quadrants at $X/h = 1.5$ (top), 4.0 (middle) and 9.0 (bottom) for the excited flow.

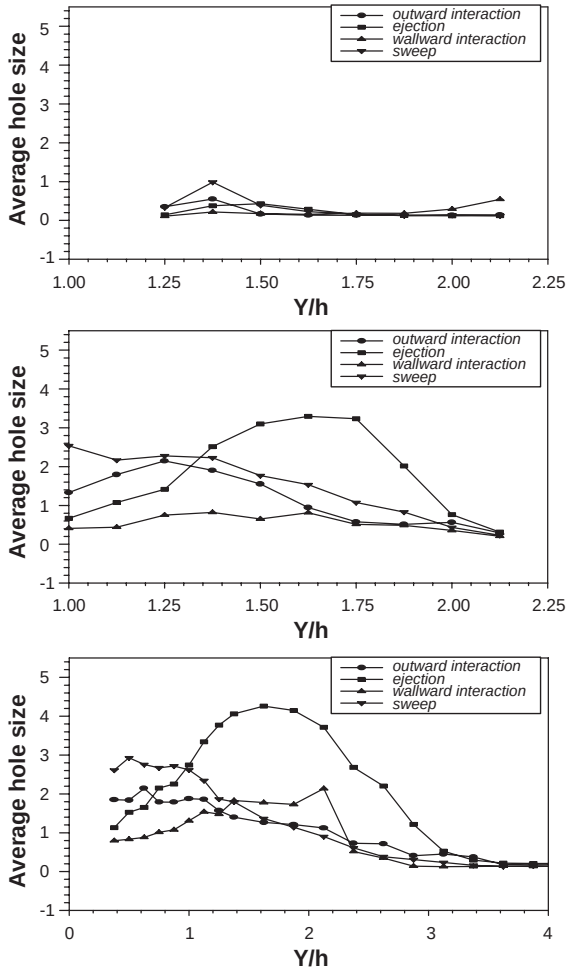

Fig. 16. The average hole size (uncertainty = ±5.0%) profile of different quadrants at $X/h = 1.5$ (top), 4.0 (middle) and 9.0 (bottom) for the unexcited flow.

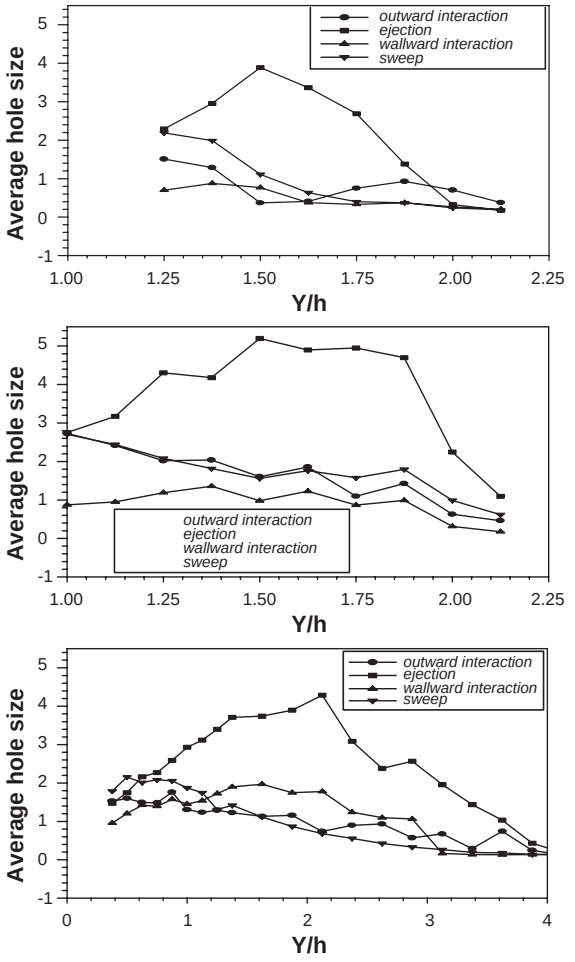

Fig. 17. The average hole size (uncertainty = ±5.0%) profile of different quadrants at $X/h = 1.5$ (top), 4.0 (middle) and 9.0 (bottom) for the excited flow.

Table 1
The comparison of Y/h locations for maximum skewness and flatness value with that for maximum average hole size of ejection motion

X/h	Y/h at maximum skewness and flatness value		Y/h at maximum ejection average hole size value	
	Unexcited case	Excited case	Unexcited case	Excited case
1.5	1.55	1.6	1.4	1.5
4.0	1.6	1.7	1.6	1.6
9.0	2.4	2.6	1.8	2.2

From the above discussion, it is observed that ejection is associated with the largest scales and the maximum hole size associated with the ejection motion is observed in the outer region of the shear layer. The skewness and flatness value presented in the previous section also peak in the outer shear layer region. Therefore, one asks the question whether the

ejection motion is related to the non-Gaussian higher-order moments. To investigate this, the Y/h locations corresponding to maximum skewness, flatness and average hole size values are shown in Table 1. Table 1 shows that the Y/h locations corresponding to the maximum value of skewness and flatness are generally quite close to the Y/h values corresponding to the maximum average hole size of the ejection motion. Thus, the higher-order moments and ejection motions are correlated, and the non-Gaussian nature of the flow in the upper regions of the shear layer is primarily due to the large-scale ejection motions.

5. Summary

The reattaching shear layer developing behind a surface-mounted rib with and without an external imposed excitation has been experimentally investigated. Due to the imposed excitation the reattachment length of the reattaching shear layer behind the rib decreases, indicating the potential of flow excitation for heat transfer enhancement. The shear stress is more for the excited flow prior to reattachment and less in the post-reattachment region, indicating insignificant total drag penalty for the excited flow. The X-momentum transport is enhanced in the near wall region due to fundamental excitation. The imposed oscillation mostly affects the coherent part of the total fluctuation.

The redeveloping flow after reattachment is distinctly different from that of a flat plate boundary layer, as the Reynolds stress correlation for the rib roughened boundary layer is smaller than that of the flat plate boundary layer. This observation is supported by the fact that the quadrant motions present behind the rib are different from what has been reported for a wall boundary layer. The skewness and flatness values are observed to depart from the respective Gaussian value of 0 and 3 in the upper part of the shear layer. This departure is attributed to the presence of predominant large-scale ejection motions in the outer edge of the shear layer. The ejection motion has the highest contribution to the total shear stress production and also has the largest eddy size among all the quadrant motions.

References

Acharya, S., Myrum, T.A., Dutta, S., 1998. Heat transfer in turbulent flow past a surface-mounted two-dimensional rib. ASME Journal of Heat Transfer 120, 550–562.

Acharya, S., Myrum, T.A., Inamdar, S., 1991. Subharmonic excitation of the shear layer between two ribs: vortex interaction and pressure field. AIAA Journal 29, 1390–1399.

Antonia, R.A., Luxton, R.E., 1971. The response of a turbulent boundary layer to a step change in surface roughness. Journal of Fluid Mechanics 48, 721–761.

Arnal, M., Friedrich, R., 1991. The instantaneous structure of a turbulent flow over a back-ward facing step. Separated Flows and Jets, IUTAM Symposium Novosibirsk/USSR, pp. 709–717.

Bogard, D.G., Tiederman, W.G., 1987. Characteristics of ejections in turbulent channel flow. Journal of Fluid Mechanics 179, 1–19.

Chandrsuda, C., Bradshaw, P., 1981. Turbulence structure of a reattaching mixing layer. Journal of Fluid Mechanics 110, 171–194.

Durao, D.F.G., Gouveia, P.S.T., Pereira, J.C.F., 1991. Velocity characteristics of the flow around a square cross section cylinder placed near a channel wall. Experiments in Fluids 11, 341–350.

Durbin, P., Reif, P., 2001. Statistical Theory and Modeling for Turbulent Flow. Wiley, New York.

Fiedler, H.E., Mensing, P., 1985. The plane turbulent shear layer with periodic excitation. Journal of Fluid Mechanics 150, 281–309.

Hasan, M.A.Z., 1992. The flow over a backward facing step under controlled perturbation: laminar separation. Journal of Fluid Mechanics 238, 73–96.

Ho, C.M., Huere, P., 1984. Perturbed free shear layers. Annual Review of Fluid Mechanics 16, 365–424.

Liou, T.M., Kao, C.F., 1988. Symmetric and asymmetric turbulent flows in a rectangular duct with a pair of ribs. ASME Journal of Fluids Engineering 110, 373–379.

Luchik, T.S., Tiederman, W.G., 1987. Time scale and structure of ejections and bursts in turbulent channel flows. Journal of Fluid Mechanics 174, 529–552.

Moffat, R.J., 1982. Contributions to the theory of single-sample uncertainty analysis. ASME Journal of Fluids Engineering 104, 250–260.

Myrum, T.A., Qiu, X., Acharya, S., 1993. Heat transfer enhancement in a ribbed duct using vortex generators. International Journal of Heat and Mass Transfer 36, 3497–3508.

Panigrahi, P.K., Acharya, S., 1996. Spectral characteristics of separated flow behind a surface mounted square rib. 27th AIAA Fluid Dynamics Conference, AIAA Paper, pp. 96–1931.

Panigrahi, P.K., Acharya, S., 1999. Mechanisms of turbulence transport in a turbine blade coolant passage with a rib turbulator. ASME Journal of Turbomachinery 121, 152–159.

Tropea, C.D., Gackstatter, R., 1985. The flow over two-dimensional surface-mounted obstacles at low Reynolds number. ASME Journal of Fluids Engineering 107, 489–494.

Wallace, J.M., Eckelmann, H., Brodkey, R.S., 1972. The wall region in turbulent shear flow. Journal of Fluid Mechanics 54, 39–48.

Willmarth, W.W., Lu, S.S., 1972. Structure of the Reynolds stress near the wall. Journal of Fluid Mechanics 55, 65–92.

Zhou, M.D., Heine, C., Wygnanski, I., 1996. The effects of excitation on the coherent and random motion in a plane wall jet. Journal of Fluid Mechanics 310, 1–37.